

Supporting Information for

Combined high alkalinity and pressurization enable efficient CO₂ electroreduction to CO

Christine M. Gabardo, Ali Seifitokaldani, Jonathan P. Edwards, Cao-Thang Dinh, Thomas Burdyny, Md Golam Kibria, Colin P. O'Brien, Edward H. Sargent and David Sinton

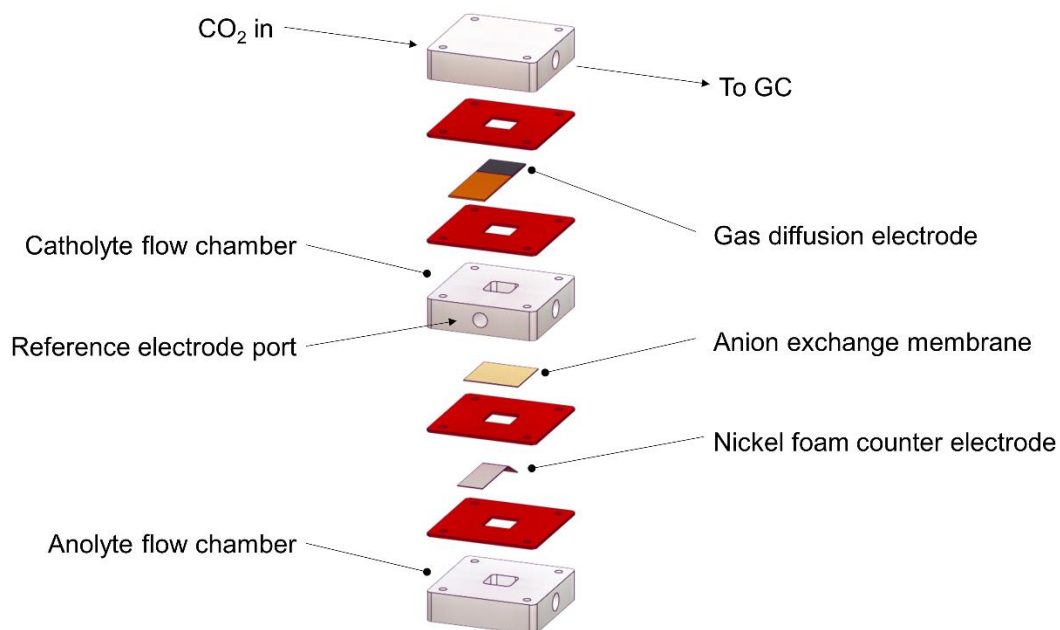


Fig S1. Schematic of flow cell electrolyzer used for CO₂RR experiments.

Concentration of KOH	1 atm		3 atm		5 atm		7 atm	
	Resistance (ohm)	pH						
1M	3.90	12.42	3.94	11.28	4.04	10.77	4.01	10.50
5M	1.35	14.49	1.30	14.32	1.44	14.21	1.45	14.12
7M	1.25	14.73	1.33	14.64	1.24	14.58	1.21	14.54
10M	1.48	14.94	1.40	14.90	1.35	14.87	1.32	14.85

Table S1: Resistance (measured through EIS) and pH (calculated based on “Modeling of CO₂ diffusion into the liquid electrolyte and local pH calculation” located later in this document).

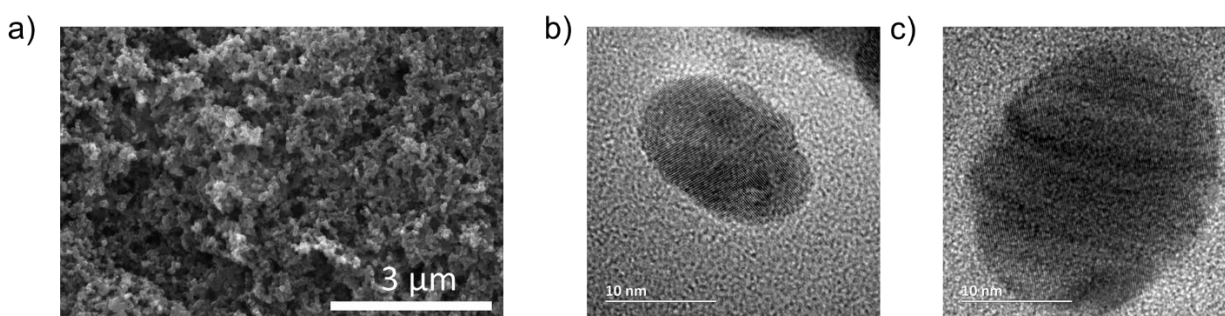


Fig S2. Typical a) SEM image of carbon gas diffusion layer before catalyst deposition and typical TEM images of the polycrystalline nanoparticle Ag catalyst, b) after CO₂RR in 1 M KOH and c) after CO₂RR in 10M KOH.

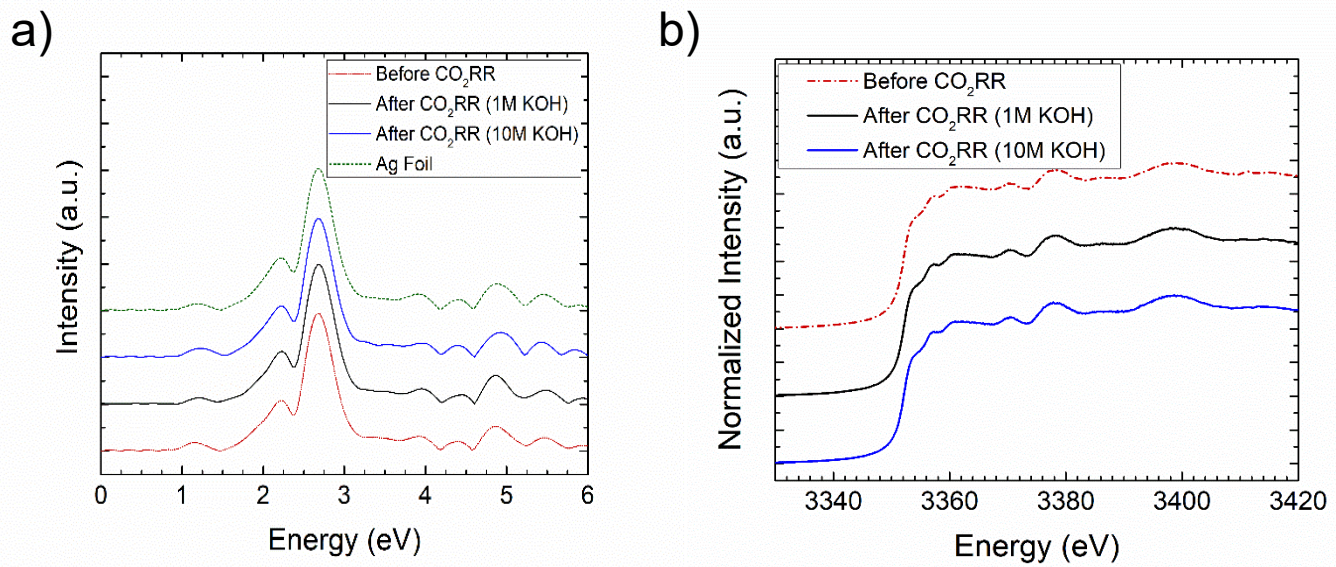


Fig S3. XAS characterization of Ag catalyst before and after CO₂RR. a) Fourier transforms (FT) of the Ag K-edge EXAFS spectra. b) L3-edge of Ag catalyst on GDE before experiments, immediately after running in 1M KOH and also immediately after running in 10M KOH. These results show that silver is very stable in alkaline media and there is neither noticeable changes in its electronic structure nor in its coordination number after running the reaction in alkaline media.

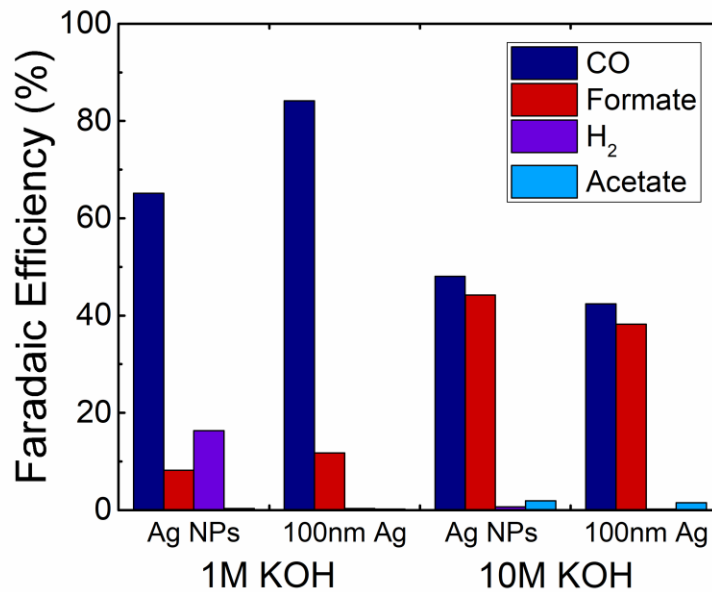


Fig S4. Comparison between silver nanoparticles (Ag NPs) and our 100nm Ag catalyst at 1M and 10M KOH, 1 atm, 300 mA/cm².

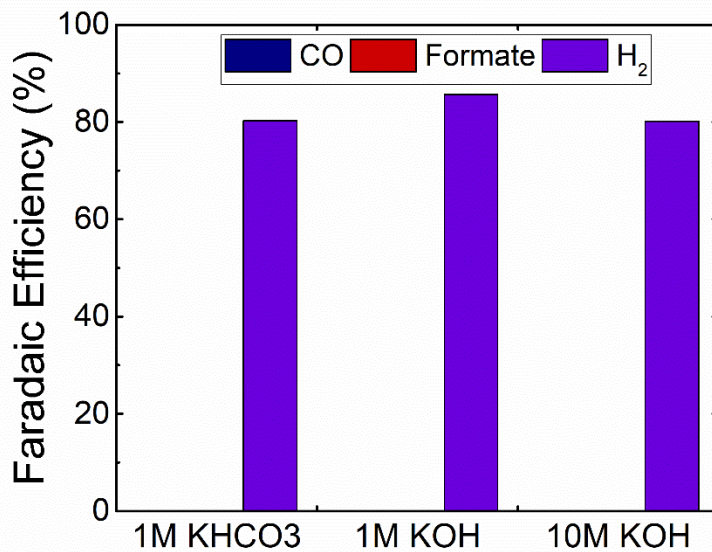


Fig S5. CO₂RR experiments in various electrolytes under nitrogen (N₂) streams at 1 atm, 300 mA/cm². Hydrogen detected at >80% FE, remaining hydrogen lost as bubbles in electrolyte.

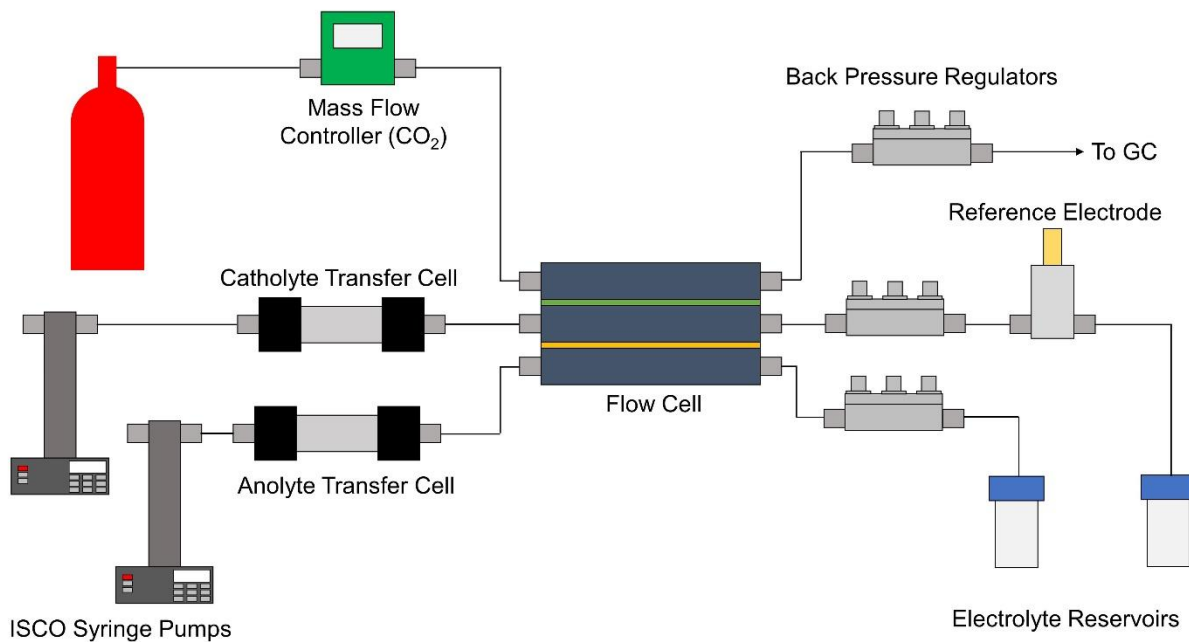


Fig S6. Schematic of setup for pressurized experiments.

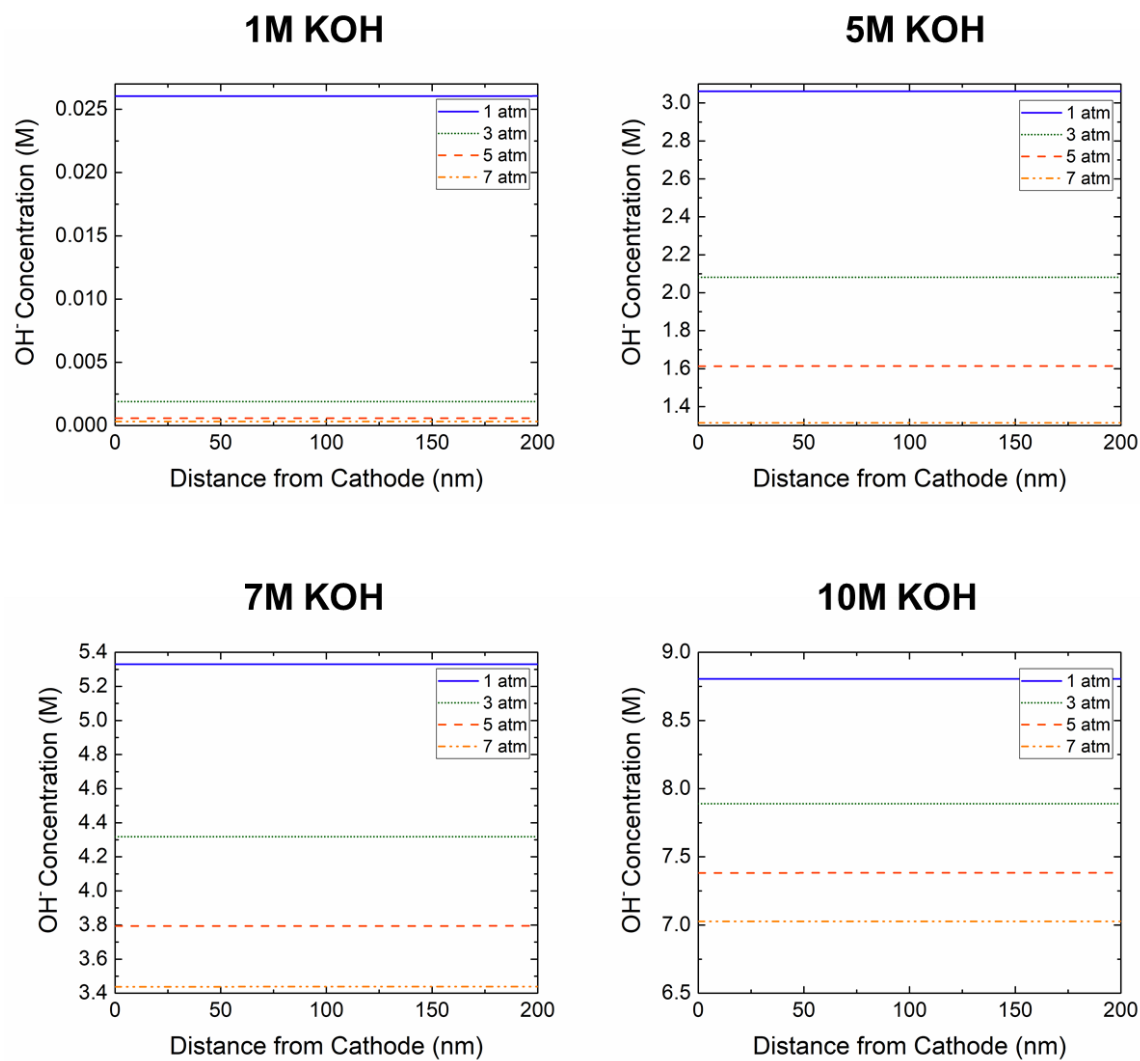


Fig S7. The OH⁻ concentration calculated based on “Modeling of CO₂ diffusion into the liquid electrolyte and local pH calculation” located later in this document.

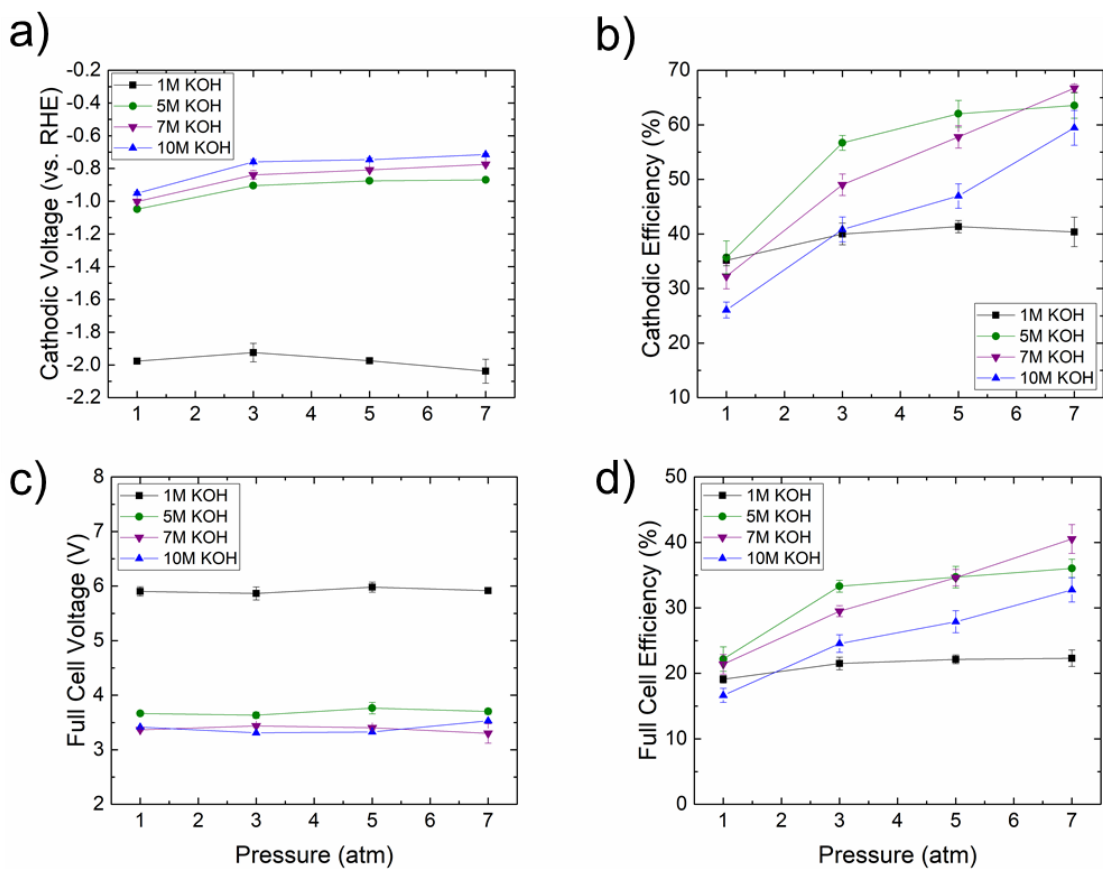


Fig S8. The a) cathodic voltage (non-iR corrected) and corresponding b) cathodic efficiency for various KOH concentrations and pressures. The a) full cell voltage (non-iR corrected) and corresponding b) full cell efficiency for various KOH concentrations and pressures. Note: the distance between anode and cathode compartments is 9.5 mm.

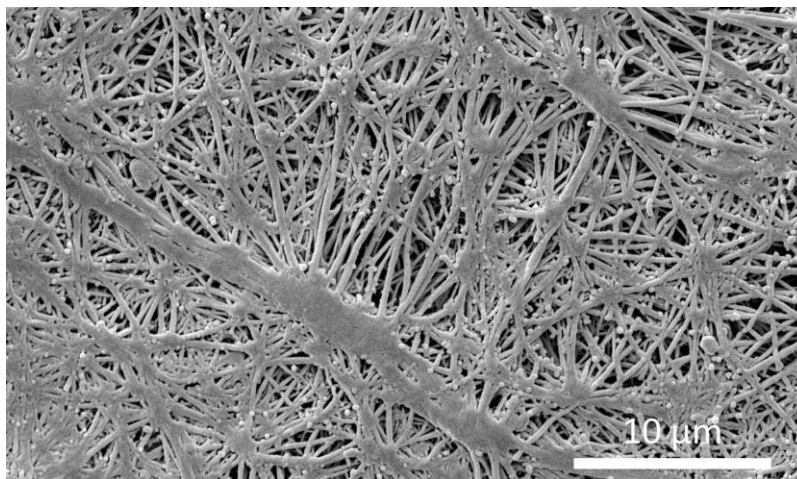


Fig S9. SEM image of the modified electrode structure for stability testing made from a PTFE membrane sputter-coated with silver.

Table S2. Data and references from Fig 4. (a) for previous CO₂RR to CO reports at high current densities.

No. in Graph Fig 4. (a)	Pressure	Electrolyte	Catalyst	Current Density (mA/cm ²)	Cathodic Efficiency (%)	Reference
1a	7 atm	7M KOH	100 nm Ag	200	80.9	This work
1b	7 atm	7M KOH	100 nm Ag	300	81.5	
1c	7 atm	7M KOH	100 nm Ag	400	76.6	
2	1 atm	1M KOH	100 nm Ag	300	54.6	
3	1 atm	1M KOH	Ag/MWCNT	350	63.6	Kenis, J. Mater. Chem. A, 2016. ¹
4	20 atm	0.5M KHCO ₃	Dropcast Ag	300	64.0	Sakata, Bull. Chem. Soc. Japan, 1997. ²
5	20 atm	0.5M KHCO ₃	Dropcast Pd	300	40.3	
6	1 atm	3M KOH	Ag NPs	230	69.6	Kenis, PCCP, 2016. ³
7	1 atm	3M KOH	Ag NPs	400	61.0	
8	1 atm	1M KOH	Ag/TiO ₂	101	61.6	Kenis, ChemSusChem, 2014. ⁴
9	30 atm	0.1M KHCO ₃	Rh Wire	163	41.9	Sakata, J. Electroanal Chem., 1995. ⁵
10	30 atm	0.1M KHCO ₃	Ag Wire	163	50.2	
11	30 atm	0.1M KHCO ₃	Au Wire	163	47.2	
12	1 atm	2M KOH	MWNT/PyPBI/Au	101	80.7	Kenis, ACS Energy Lett., 2018. ⁶
13	1 atm	2M KOH	MWNT/PyPBI/Au	186	65.4	
14	1 atm	2M KOH	MWNT/PyPBI/Au	319	45.3	

Calculation of Cathodic and Full Cell Voltage Efficiency (VE) & Cathodic and Full Cell Energetic Efficiency (EE)

$$\text{Cathodic Voltage Efficiency: } VE_{cathodic} = \frac{1.23+(-E_{CO})}{1.23+(-E_{cathode})} \quad (\text{Eq. S1})$$

$$\text{Full Cell Voltage Efficiency: } VE_{full\ cell} = \frac{1.23+(-E_{CO})}{(E_{full\ cell})} \quad (\text{Eq. S2})$$

$$\text{CO Cathodic Energetic Efficiency: } EE_{cathodic} = VE_{cathodic} \times FE_{CO} \quad (\text{Eq. S3})$$

$$\text{CO Full Cell Energetic Efficiency: } EE_{full\ cell} = VE_{full\ cell} \times FE_{CO} \quad (\text{Eq. S4})$$

where $E_{cathode}$ is the applied cathode potential vs RHE; $E_{full\ cell}$ is the full cell applied potential; $E_{CO} = -0.109\text{ V}$ is thermodynamic potential (vs RHE) of CO_2 reduction to CO; FE_{CO} is the measured CO Faradaic efficiency as a percentage.

Modeling of CO_2 diffusion into the liquid electrolyte and local pH calculation.

A reaction-diffusion model was used to determine the local pH of the electrode under various operating conditions including pressurization and different bulk KOH concentrations. The predicted pH values of the electrode were then used to account for the Nernst shift in the working electrode potentials when calculating the potential versus a reversible hydrogen electrode. The predicted pH values, shown in Table S1 for all cases, were calculated at a current of 0 mA/cm^2 .

The reaction-diffusion model is similar to the 1D model previously,⁷ but with additional pressure effects. The equations used, and bounds of the model, are presented here for completeness. The diffusion of CO_2 into the electrolyte was modeled taking into account equilibrium between the active species CO_2 , OH^- , HCO_3^- and CO_3^{2-} . A gas-liquid interface was assumed at $x = 0\ \mu\text{m}$ where the CO_2 concentration was assumed to be equal to the saturated state at various KOH concentrations⁸ and pressures. A liquid diffusion boundary was assumed at $x = 500\ \mu\text{m}$ where the concentrations of all aqueous species were assumed to be equal to that of the bulk electrolyte.

From the experimental results a catalyst layer thickness, $L_{catalyst}$, of 100 nm is assumed, extending from $x = 0\ \mu\text{m}$ to $x = 0.1\ \mu\text{m}$ with an assumed porosity, ϵ , of 60%. Also based on the experimental results, a product selectivity of 100% CO + Formate (both consume 2 electrons), was assumed ($FE_{CO}+FE_{HCOOH} = 1$ and $n_{e,CO} = n_{e,HCOOH} = 2$). The choice of selectivity affects the

relative amount of CO₂ consumed per electron transferred as well as the H⁺ consumed, and subsequently, OH⁻ generated through water dissociation at the catalyst surface.

The diffusion equations are adapted from previous CO₂ reduction models in neutral media and account for CO₂ consumption, bicarbonate-carbonate equilibrium and the generation of OH⁻ inside the catalyst layer.^{9,10}

$$\frac{\partial[CO_2]}{\partial t} = D_{CO_2} \frac{\partial^2[CO_2]}{\partial x^2} - [CO_2][OH^-]k_{1f} + [HCO_3^-]k_{1r} - R_{CO_2} \quad (\text{Eq. S5})$$

$$\frac{\partial[HCO_3^-]}{\partial t} = D_{HCO_3^-} \frac{\partial^2[HCO_3^-]}{\partial x^2} + [CO_2][OH^-]k_{1f} - [HCO_3^-]k_{1r} - [HCO_3^-][OH^-]k_{2f} + [CO_3^{2-}]k_{2r} \quad (\text{Eq. S6})$$

$$\frac{\partial[CO_3^{2-}]}{\partial t} = D_{CO_3^{2-}} \frac{\partial^2[CO_3^{2-}]}{\partial x^2} + [HCO_3^-][OH^-]k_{2f} - [CO_3^{2-}]k_{2r} \quad (\text{Eq. S7})$$

$$\frac{\partial[OH^-]}{\partial t} = D_{OH^-} \frac{\partial^2[OH^-]}{\partial x^2} - [CO_2][OH^-]k_{1f} + [HCO_3^-]k_{1r} - [HCO_3^-][OH^-]k_{2f} + [CO_3^{2-}]k_{2r} + R_{OH} \quad (\text{Eq. S8})$$

All CO₂ reduction reactions are assumed to occur homogeneously within the 100 nm catalyst layer (from $x = 0 \mu\text{m}$ to $x = 0.1 \mu\text{m}$). The consumption of CO₂ and production of hydroxide are then calculated as:

$$R_{CO_2} = \begin{cases} \frac{j}{F} \left(\frac{FE_{CO}}{n_{e,CO}} + \frac{FE_{CHOOH}}{n_{e,CHOOH}} \right) \frac{\epsilon}{L_{catalyst}} & , \quad 0 \leq x \leq L_{catalyst} \\ 0 & , \quad x > L_{catalyst} \end{cases} \quad (\text{Eq. S9})$$

$$R_{OH} = \begin{cases} \frac{j}{F} \frac{\epsilon}{L_{catalyst}} & , \quad 0 \leq x \leq L_{catalyst} \\ 0 & , \quad x > L_{catalyst} \end{cases} \quad (\text{Eq. S10})$$

All equilibrium and rate constants in Eq. S5-S8 are calculated as a function of temperature and salinity as discussed previously.¹⁰

Simulations were performed by prescribing current density, bulk KOH concentration and pressure. The output of the simulation was a concentration profile of CO₂ and OH⁻ as a function of electrolyte penetration depth from the left-hand boundary. The predicted pH used in Table S1 was calculated as the average pH within the catalyst layer.

Pressurization Energy

A frequent concern with pressurized systems is the energy required to pressurize the reactants. This section estimates the energy for the current system and compares it to the electrical energy, via reduction in overpotentials, saved through pressurization. For comparison they are tabulated per kg of CO₂ converted.

Assumptions:

- CO₂ behaves as an ideal gas
- CO₂ enters the compressor at 298 K, 1 atm (state 1) and is pressurized to 7 atm (state 2)
- The compressor has an isentropic efficiency of 50%
- The CO₂ utilization rate in the reaction is 3% (to be consistent with the experiments presented, a real system would likely boast a much higher value)

The first step is to calculate the entropy at state 2 if the process occurs isentropically:

$$s_2^o = s_1^o + R \ln \frac{P_2}{P_1} = 213.7 \frac{\text{kJ}}{\text{kmol K}} + \left(8.314 \frac{\text{kJ}}{\text{kmol K}} \right) \ln(7) = 229.9 \frac{\text{kJ}}{\text{kmol K}}$$

Based on this value, we enter the thermodynamic tables and determine that the enthalpy at the outlet of the compressor for the isentropic process is 15.35 kJ/kmol.¹¹ From those same tables at 298 K the enthalpy for CO₂ is 9.364 kJ/kmol. Considering the compressor and reaction inefficiencies will increase the amount of energy required to run the compressor yielding:

$$w_{\text{compressor}} = \frac{h_{2,s} - h_1}{\eta_{\text{compressor}} \eta_{\text{utilization}}} = \frac{15.35 - 9.364 \frac{\text{kJ}}{\text{kmol}}}{(0.50)(0.03)} = 399 \frac{\text{kJ}}{\text{kmol}} * \frac{1 \text{ kmol}}{44.01 \text{ kg}} = \mathbf{9.07 \frac{\text{kJ}}{\text{kg}}}$$

The overpotential of the most efficient 7 atm condition (7 M KOH) is 400 mV less than that of the most efficient 1 atm condition (1 M KOH). From this information, the electrical energy saved in the two electron reaction from CO₂ to CO is:

$$w_{\text{electrical}} = zFE = \left(2 \frac{\text{mol } e}{\text{mol CO}_2} \right) \left(96485 \frac{\text{C}}{\text{mol } e} \right) \left(0.400 \frac{\text{J}}{\text{C}} \right) * \left(\frac{1 \text{ mol CO}_2}{44.01 \text{ g}} \right) = 1750 \frac{\text{J}}{\text{g}} = \mathbf{1750 \frac{\text{kJ}}{\text{kg}}}$$

From this it can be seen that the energy savings from the reduced overpotentials drastically outweigh those from the associated compression energy; they are orders of magnitude apart even with the rather abysmal reaction and compressor efficiencies selected.

References

- 1 S. Ma, R. Luo, J. I. Gold, A. Z. Yu and P. J. A. Kenis, *J. Mater. Chem. A*, 2016, **4**, 8573–8578.
- 2 K. Hara and T. Sakata, *Bull. Chem. Soc. Jpn.*, 1997, **70**, 571–576.
- 3 S. Verma, X. Lu, S. Ma, R. I. Masel and P. J. A. Kenis, *Phys. Chem. Chem. Phys.*, 2016, **18**, 7075–7084.
- 4 S. Ma, Y. Lan, G. M. J. Perez, S. Moniri and P. J. A. Kenis, *ChemSusChem*, 2014, **7**, 866–874.
- 5 K. Hara, A. Kudo and T. Sakata, *J. Electroanal. Chem.*, 1995, **391**, 141–147.
- 6 S. Verma, Y. Hamasaki, C. Kim, W. Huang, S. Lu, H.-R. M. Jhong, A. A. Gewirth, T. Fujigaya, N. Nakashima and P. J. A. Kenis, *ACS Energy Lett.*, 2018, **3**, 193–198.
- 7 A. Seifitokaldani, C. M. Gabardo, T. Burdyny, C. Dinh, J. P. Edwards, M. G. Kibria, O. S. Bushuyev, S. O. Kelley, D. Sinton and E. H. Sargent, *J. Am. Chem. Soc.*, 2018, jacs.7b13542.
- 8 S. Weisenberger and A. Schumpe, *AIChE J.*, 1996, **42**, 298–300.
- 9 M. R. Singh, E. L. Clark and A. T. Bell, *Phys. Chem. Chem. Phys.*, 2015, **17**, 18924–18936.
- 10 T. Burdyny, P. J. Graham, Y. Pang, C. T. Dinh, M. Liu, E. H. Sargent and D. Sinton, *ACS Sustain. Chem. Eng.*, 2017, **5**, 4031–4040.
- 11 M. J. Moran, H. N. Shapiro, D. D. Boettner and M. B. Bailey, *Fundamentals of Engineering Thermodynamics*, John Wiley & Sons Inc., Hoboken, NJ, 8th edn., 2014.